

Article

Phase-Controlled Absorption and Dispersion Properties of a Multi-Level Quantum Emitter Interacting with Bismuth-Chalcogenide Microparticles

Theodoros Papachronis ¹, Nikolaos Kyvelos ^{1,2}, Emmanuel Paspalakis ³  and Vassilios Yannopoulos ^{1,*} 

¹ Department of Physics, School of Applied Mathematical and Physical Sciences, National Technical University of Athens, GR-15780 Athens, Greece; tpapachronis@gmail.com (T.P.); niky@mci.sdu.dk (N.K.)

² POLIMA—Center for Polariton-Driven Light–Matter Interactions, University of Southern Denmark, Campusvej 55, DK-5230 Odense M, Denmark

³ Department of Materials Science, University of Patras, GR-26504 Patras, Greece; paspalak@upatras.gr

* Correspondence: vyannop@mail.ntua.gr

Abstract: We theoretically study the impact of bismuth-chalcogenide microparticles on the linear absorption and dispersion properties of a four-level double-V-type quantum system. The quantum system interacts with two circularly polarized laser fields of the same frequency but with different phases and electric field amplitudes. Our study indicates that the inclusion of bismuth-chalcogenide microparticles leads to notable alterations in the absorption and dispersion spectra corresponding to one of the probe laser fields (while both fields are present). These alterations are much more dramatic compared to those induced by common plasmonic materials. By manipulating the field amplitudes as well as the phase difference between the two incident waves, the optical properties of the system can be efficiently controlled. Our study also highlights several effects, including complete optical transparency, zero absorption with nonzero dispersion, and gain without inversion.

Keywords: quantum interference; spontaneous emission; polar materials



Citation: Papachronis, T.; Kyvelos, N.; Paspalakis, E.; Yannopoulos, V. Phase-Controlled Absorption and Dispersion Properties of a Multi-Level Quantum Emitter Interacting with Bismuth-Chalcogenide Microparticles. *Photonics* **2023**, *10*, 1296. <https://doi.org/10.3390/photonics10121296>

Received: 1 October 2023

Revised: 21 November 2023

Accepted: 22 November 2023

Published: 24 November 2023



Copyright: © 2023 by the authors. Licensee MDPI, Basel, Switzerland. This article is an open access article distributed under the terms and conditions of the Creative Commons Attribution (CC BY) license (<https://creativecommons.org/licenses/by/4.0/>).

1. Introduction

Quantum plasmonics is an area of research that involves the intersection of plasmonics and quantum mechanics [1–4]. Plasmonics is the study of the collective electron oscillations in metal-like structures, while quantum mechanics is used to manipulate and control light at the nanoscale. This combination presents new possibilities for high-resolution imaging, biosensing, and the development of ultra-small optical devices [5]. One of the main aspects of quantum plasmonics is the use of quantum entanglement, which allows for the correlation of quantum states of multiple particles, leading to promising applications in quantum computing, cryptography, and communication. Overall, the integration of quantum plasmonics and quantum nanophotonics is a promising avenue for technological advancements in the fields of nanophotonics and quantum technologies [6].

The success of quantum technologies that utilize plasmonic devices is contingent upon the establishment of an efficient coherent interaction between light and a quantum emitter (QE). One effective strategy for enhancing this interaction is to integrate the QE with a plasmonic structure, which can modify the spontaneous emission (SE) rates by means of the local electromagnetic density of states (LDOS) available to the emitter. This phenomenon, known as the Purcell effect [7], is widely regarded as a crucial aspect of quantum plasmonics. To quantify the change in the SE rate of the QE, the Purcell factor is used to compare the rate in the presence of a photonic or plasmonic environment to the SE rate of the QE in a vacuum. The Purcell effect has been extensively studied in the literature and is well-established as a key factor in the successful implementation of quantum plasmonics [8,9].

Noble metals, such as silver, gold, and copper, are the most widely-used materials for plasmon excitations, but their high intrinsic losses have prompted research into alternative materials. High-index dielectrics and semiconductors, including Si, GaAs, and AlGaAs, have been suggested as possible alternatives due to their potential for mitigating losses [10]. The use of high-refractive-index materials in plasmonics offers numerous benefits, including improved light-matter interactions, reduced losses, and compatibility with silicon-based electronics [11]. As a result, the field of plasmonics with high-refractive-index materials is rapidly expanding and holds great promise for applications in sensing, photonics, and quantum computing [12].

Chalcogenides are a group of materials containing elements like sulfur, selenium, and tellurium that exhibit excellent dielectric properties owing to their robust phonon resonances in the THz range. These materials have been the focus of significant interest for their unique electronic and optical properties that make them well-suited for photonics and optoelectronics [13–15]. Bismuth chalcogenides are a type of material that are highly valued in the field of nanophotonics and other optical technologies because of their impressive light confinement properties and high refractive index [16,17]. Chalcogenides have been extensively studied in recent years for their potential applications in polaritonic excitations and for enhancing light-matter interactions in quantum technologies [18].

Bismuth chalcogenides are of particular interest for their ability to exhibit strong coupling between light and matter through polaritonic excitations. Unlike noble-metal nanostructures, which can have high Purcell factors but suffer from large ohmic losses [19] that hinder their coupling with quantum emitters, bismuth chalcogenides have lower losses and higher field enhancement, making them a promising candidate for efficient QE coupling. These materials generate high partially local density of states (PLDOS) due to polaritonic excitations [20–22], resulting in significant modifications and control over the SE rate of nearby QEs [23]. This unique property opens up opportunities for a range of applications in areas such as photonics, sensing, and quantum information processing.

The present work studies the Purcell effect in a double V-type quantum system. Such few-level quantum systems are simplified models that capture specific features while leaving out some of the complexity present in actual atomic systems. Here, we focus on how the phase difference between two applied laser fields affects the optical properties, specifically the real and imaginary parts of the electric susceptibility of a 4-level double V-type quantum emitter near bismuth-chalcogenide microparticles. One V-type transition in the system is affected by the microparticles while the other interacts with a free-space vacuum. Our study utilizes a density matrix methodology to calculate the linear susceptibility and demonstrates that the presence of the microparticles strongly modifies the absorption and dispersion spectra of the laser fields. Furthermore, we demonstrate that by manipulating the relative ratio of the electric-field amplitudes as well as the phase difference between the two probe waves, the optical properties of the system can be controlled efficiently. The present study also reveals some exotic phenomena such as optical transparency, zero absorption with non-zero dispersion, and gain without inversion, and identifies the specific conditions that give rise to these phenomena.

We note that the analysis presented below is based on earlier work where four-level quantum systems are placed in plasmonic nanostructures [24,25]. We stress that the cases of plasmonic nanostructures and bismuth-chalcogenide microstructures have significant differences when influencing the quantum interference of nearby QEs. Plasmonic nanostructures can give significant enhancement of quantum interference due to surface-plasmon excitations, but this happens in the visible part of the spectrum and not in the THz regime which is studied here for the case of bismuth-chalcogenide microstructures. Also, for the plasmonic nanostructures, the enhancement is found for significantly smaller distances, typically only for few tens of nanometers from the surface of the relevant plasmonic nanostructure, and certainly not for few micrometers from the surface that we present here.

2. Theory

The quantum emitter under study is presented schematically in Figure 1. The system being studied is a four-level structure that contains two nearby upper states, denoted as $|2\rangle$ and $|3\rangle$, and two lower states $|0\rangle$ and $|1\rangle$. This configuration is referred to as a double-V-type system, which helps to distinguish between two distinct three-level V-type transitions present in the system. We use the states $|2\rangle$ and $|3\rangle$ to represent two sublevels with Zeeman splitting. Then, the dipole moment operator is taken as $\vec{\mu} = \mu'(|2\rangle\langle 0|\hat{\epsilon}_- + |3\rangle\langle 0|\hat{\epsilon}_+) + \mu(|2\rangle\langle 1|\hat{\epsilon}_- + |3\rangle\langle 1|\hat{\epsilon}_+) + \text{H.c.}$, where $\hat{\epsilon}_{\pm} = (\mathbf{e}_z \pm i\mathbf{e}_x)/\sqrt{2}$, describe the right-rotating ($\hat{\epsilon}_+$) and left-rotating ($\hat{\epsilon}_-$) unit vectors and μ, μ' are taken to be real. A similar model has been used in refs. [24–27].

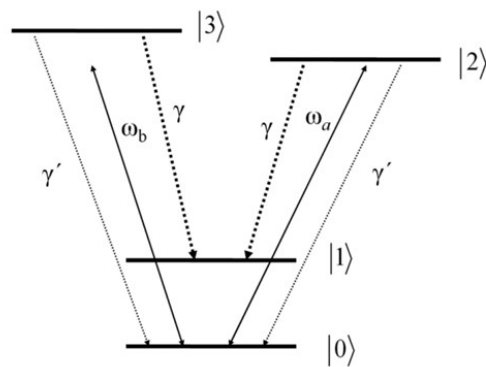


Figure 1. The quantum emitter studied throughout this work. It is a double-V-type emitter containing two upper states $|2\rangle$ and $|3\rangle$ which decay spontaneously to the two lower states $|0\rangle$ and $|1\rangle$. The system additionally engages with two weak probe electromagnetic fields, both of which are circularly polarized and share the same angular frequency, denoted as $\omega_a = \omega_b$. The field denoted by a drives the transition $|0\rangle$ to $|2\rangle$ whilst the field denoted by b drives the transition $|0\rangle$ to state $|3\rangle$.

The system is influenced by two circularly polarized laser fields of continuous wave nature, with a combined electric field provided by

$$\vec{E}(t) = \hat{\epsilon}_+ E_a \cos(\omega_a t + \phi_a) + \hat{\epsilon}_- E_b \cos(\omega_b t + \phi_b). \tag{1}$$

Here, E_a and E_b are the electric field amplitudes. The parameters ω_a and ω_b are the angular frequencies of the laser fields. Also, the phases of the fields are denoted as ϕ_a and ϕ_b . As we noted above, the laser field a drives the transition from $|0\rangle$ to state $|2\rangle$ and the laser field b drives the transition from $|0\rangle$ to $|3\rangle$. We take both fields having equal frequencies $\omega_a = \omega_b = \omega$. We employ the dipole and rotating wave approximations and obtain the Hamiltonian that describes the interaction between the quantum system and the laser fields, which is expressed as

$$H = \hbar\left(-\delta - \frac{\omega_{32}}{2}\right)|2\rangle\langle 2| + \hbar\left(-\delta + \frac{\omega_{32}}{2}\right)|3\rangle\langle 3| - \left(\frac{\hbar\Omega_a e^{i\phi_a}}{2}|0\rangle\langle 2| + \frac{\hbar\Omega_b e^{i\phi_b}}{2}|0\rangle\langle 3| + \text{H.c.}\right). \tag{2}$$

Here, $\delta = \omega - \tilde{\omega}$ denotes the detuning from resonance with the average transition energies of states $|2\rangle$ and $|3\rangle$ from state $|0\rangle$, with $\tilde{\omega} = (\omega_3 + \omega_2)/2 - \omega_0$, $\omega_{32} = (\omega_3 - \omega_2)/2$. Furthermore, Ω_a and Ω_b represent the Rabi frequencies corresponding to fields a and b , respectively. These frequencies are defined as $\Omega_a = \mu' E_a/\hbar$ and $\Omega_b = \mu' E_b/\hbar$. In addition, $\hbar\omega_n$ where $n = 0, 1, 2, 3$, corresponds to the energy level of state $|n\rangle$. We stress that the Hamiltonian in Equation (2) only accounts for the interaction between the quantum system and the external laser fields.

However, the quantum system also interacts with the vacuum and undergoes SE. The details of the calculations of the inclusion of SE in the system is lengthy and will not be

presented here. We refer the readers to ref. [25] where the details of the calculations are provided. Both excited states $|2\rangle$ and $|3\rangle$ decay spontaneously to state $|0\rangle$ with decay rates $2\gamma'_2, 2\gamma'_3$, respectively, and to state $|1\rangle$ with decay rates $2\gamma_2, 2\gamma_3$, respectively. We assume that transitions from states $|2\rangle$ and $|3\rangle$ to state $|1\rangle$ occur through surface phonon-polariton resonances of the nearby bismuth-chalcogenide microparticles, while the frequencies of the transitions to state $|0\rangle$ are far away from phonon-polariton resonances and are therefore not influenced by the microparticles. Therefore, the decay from states $|2\rangle$ and $|3\rangle$ to state $|0\rangle$ occurs due to the interaction of the quantum system with the regular vacuum. The energy difference between states $|2\rangle$ and $|3\rangle$ is chosen to be small, such that ω_{32} is typically a few Γ_0 , where Γ_0 is the decay rate of states $|2\rangle$ and $|3\rangle$ to state $|1\rangle$ in vacuum, and is assumed to be equal for both states. We can therefore take that $\gamma_2 = \gamma_3 = \gamma$ and $\gamma'_2 = \gamma'_3 = \gamma'$ [28].

Using the Hamiltonian as described in Equation (2) and including the interaction with the vacuum modes [25], we formulate the equations for the density matrix components of the system, in the Markovian approximation,

$$\begin{aligned} \dot{\rho}_{00}(t) &= 2\gamma'[\rho_{22}(t) + \rho_{33}(t)] - i\frac{\Omega_a}{2} [\rho_{02}(t)e^{-i\phi_a} - \rho_{20}(t)e^{i\phi_a}] \\ &\quad - i\frac{\Omega_b}{2} [\rho_{03}(t)e^{-i\phi_b} - \rho_{30}(t)e^{i\phi_b}], \end{aligned} \tag{3}$$

$$\begin{aligned} \dot{\rho}_{22}(t) &= -2(\gamma + \gamma')\rho_{22}(t) + i\frac{\Omega_a}{2} [\rho_{02}(t)e^{-i\phi_a} - \rho_{20}(t)e^{i\phi_a}] \\ &\quad - \kappa[\rho_{23}(t) + \rho_{32}(t)], \end{aligned} \tag{4}$$

$$\begin{aligned} \dot{\rho}_{33}(t) &= -2(\gamma + \gamma')\rho_{33}(t) + i\frac{\Omega_b}{2} [\rho_{03}(t)e^{-i\phi_b} - \rho_{30}(t)e^{i\phi_b}] \\ &\quad - \kappa[\rho_{23}(t) + \rho_{32}(t)], \end{aligned} \tag{5}$$

$$\begin{aligned} \dot{\rho}_{20}(t) &= (i\delta + i\frac{\omega_{32}}{2} - \gamma - \gamma')\rho_{20}(t) + i\frac{\Omega_a}{2} e^{-i\phi_a} [\rho_{00}(t) - \rho_{22}(t)] \\ &\quad - i\frac{\Omega_b}{2} e^{-i\phi_b} \rho_{23}(t) - \kappa\rho_{30}(t), \end{aligned} \tag{6}$$

$$\begin{aligned} \dot{\rho}_{30}(t) &= (i\delta - i\frac{\omega_{32}}{2} - \gamma - \gamma')\rho_{30}(t) + i\frac{\Omega_b}{2} e^{-i\phi_b} [\rho_{00}(t) - \rho_{33}(t)] \\ &\quad - i\frac{\Omega_a}{2} e^{-i\phi_a} \rho_{32}(t) - \kappa\rho_{20}(t), \end{aligned} \tag{7}$$

$$\begin{aligned} \dot{\rho}_{23}(t) &= (i\omega_{32} - 2\gamma - 2\gamma')\rho_{23}(t) + i\frac{\Omega_a}{2} e^{-i\phi_a} \rho_{03}(t) - i\frac{\Omega_b}{2} e^{i\phi_b} \rho_{20}(t) \\ &\quad - \kappa[\rho_{22}(t) + \rho_{33}(t)], \end{aligned} \tag{8}$$

with $\rho_{00}(t) + \rho_{11}(t) + \rho_{22}(t) + \rho_{33}(t) = 1$ and $\rho_{nm}(t) = \rho_{mn}^*(t)$. Above, we have introduced the coupling coefficient κ between upper states due to SE in a modified anisotropic vacuum [29]. This coefficient is responsible for quantum interference in SE [30].

The parameters γ and κ are defined as [31–34]

$$\gamma = \frac{1}{2}(\Gamma_{\perp} + \Gamma_{\parallel}), \tag{9}$$

$$\kappa = \frac{1}{2}(\Gamma_{\perp} - \Gamma_{\parallel}), \tag{10}$$

where $\Gamma_{\perp}, \Gamma_{\parallel}$ are SE rates for a dipole oriented perpendicular (\perp) or parallel (\parallel) to the surface of a nearby object (in our case microspheres).

The measure (degree) of quantum interference is provided by

$$p = \frac{\Gamma_{\perp} - \Gamma_{\parallel}}{\Gamma_{\perp} + \Gamma_{\parallel}}. \tag{11}$$

Maximum quantum interference in SE is given for $p = 1$ [30]. This can be accomplished by positioning the emitter in proximity to a structure that effectively suppresses Γ_{\parallel} . In

scenarios where the QE is situated in a vacuum, both Γ_{\perp} and Γ_{\parallel} are equal, and κ is zero, resulting in the absence of quantum interference within the system.

The spectrum of absorption and dispersion concerning a weak laser field denoted as a is dictated by the linear electric susceptibility, which is expressed as [35,36]

$$\chi^{(1)}(\omega) = \frac{2N\mu'}{\varepsilon_0 E_a e^{-i\phi_a}} \rho_{20}^{(1)} = \frac{2N\mu'^2 e^{i\phi_a}}{\varepsilon_0 \hbar} \frac{\rho_{20}^{(1)}}{\Omega_a}. \tag{12}$$

Here, $\rho_{20}^{(1)}$ is determined under steady-state conditions and in the first-order approximation with respect to E_a (or Ω_a). ε_0 represents the permittivity of a vacuum, and N stands for the density of quantum emitters.

We assume that both fields are weak and use time-dependent perturbation theory to obtain from Equations (2)–(7) after some algebra

$$\rho_{20}^{(1)} = \frac{i\frac{\Omega_a}{2} e^{-i\phi_a} (-i\delta + i\frac{\omega_{32}}{2} + \gamma + \gamma') - i\kappa\frac{\Omega_b}{2} e^{-i\phi_b}}{(-i\delta + i\frac{\omega_{32}}{2} + \gamma + \gamma')(-i\delta - i\frac{\omega_{32}}{2} + \gamma + \gamma') - \kappa^2}. \tag{13}$$

We replace the expression for $\rho_{20}^{(1)}$ from Equation (13) into Equation (12), resulting in

$$\chi^{(1)}(\delta) = \frac{N\mu^2}{\varepsilon_0 \hbar} \frac{\delta - \frac{\omega_{32}}{2} + i\gamma + i\gamma' - i\kappa\frac{E_b}{E_a} e^{i\phi}}{(-i\delta + i\frac{\omega_{32}}{2} + \gamma + \gamma')(-i\delta - i\frac{\omega_{32}}{2} + \gamma + \gamma') - \kappa^2}, \tag{14}$$

where $\phi = \phi_a - \phi_b$ is the phase difference between the two applied fields. When the quantum emitter lies in free space, i.e., in the absence of any nearby objects, Equation (14) becomes

$$\chi^{(1)}(\delta) = \frac{N\mu^2}{\varepsilon_0 \hbar} \frac{\delta - \frac{\omega_{32}}{2} + i\Gamma_0 + i\gamma'}{(-i\delta + \Gamma_0 + \gamma')^2 + \frac{\omega_{32}^2}{4}}. \tag{15}$$

In the presence of photonic environment such as microspheres in our case, Equation (14) may assume a more compact form by defining $A = \frac{N\mu^2}{\varepsilon_0 \hbar}$, $\tilde{\alpha} = \frac{\omega_{32}}{2}$, $\tilde{\gamma} = \gamma + \gamma'$, $x = \frac{E_b}{E_a}$, $\alpha = \alpha(\phi, x) = \kappa x \sin \phi - \tilde{\alpha}$, $\beta = \beta(\phi, x) = \tilde{\gamma} - \kappa x \cos \phi$, $\varepsilon = \tilde{\alpha}^2 + \tilde{\gamma}^2 - \kappa^2 = \tilde{\alpha}^2 + (\Gamma_{\parallel} + \gamma')(\Gamma_{\perp} + \gamma')$ (> 0) and $\zeta = -2\tilde{\gamma}$ (< 0). Evidently, by separating Equation (14) in real and imaginary parts, we obtain

$$\text{Re}[\chi^{(1)}(\delta)] = A \frac{(\alpha + \delta)(\varepsilon - \delta^2) + \beta\zeta\delta}{(\varepsilon - \delta^2)^2 + \zeta^2\delta^2}, \tag{16}$$

and

$$\text{Im}[\chi^{(1)}(\delta)] = A \frac{\beta(\varepsilon - \delta^2) - \zeta\delta(\alpha + \delta)}{(\varepsilon - \delta^2)^2 + \zeta^2\delta^2}. \tag{17}$$

3. Zero Absorption, Optical Transparency and Inversion without Gain

Under the conditions described in the previous section, the interaction of two laser fields on a quantum emitter, in a favourable photonic environment, can lead to the enhancement of quantum interference. This, in turn, can result in the observation of unusual phenomena such as zero absorption with dispersion, optical transparency, and inversion without gain.

Initially, we discuss a scenario where there is no absorption ($\text{Im}[\chi^{(1)}(\delta)] = 0$), yet dispersion is present ($\text{Re}[\chi^{(1)}(\delta)] \neq 0$). This results in an elevation of the refractive index without any concurrent absorption, as observed in [37,38]. This is observed under the condition of detunings

$$\delta_{\pm} = \frac{\tilde{\gamma}(\tilde{\alpha} - \kappa x \sin \phi) \pm \sqrt{\tilde{\gamma}^2(\tilde{\alpha} - \kappa x \sin \phi)^2 + \varepsilon(\kappa^2 x^2 \cos^2 \phi - \tilde{\gamma}^2)}}{\tilde{\gamma} + \kappa x \cos \phi}. \tag{18}$$

If the value inside the square root is zero or positive, then this results in

$$\tilde{\gamma}^2(\tilde{\alpha} - \kappa x \sin \phi)^2 \geq \varepsilon(\tilde{\gamma}^2 - \kappa^2 x^2 \cos^2 \phi). \tag{19}$$

At $\delta = 0$, or when ω equals $\tilde{\omega}$ (a frequency at which the system exhibits pronounced reduction in absorption when subjected to a linearly polarized laser field, as reported in [39]), Equation (18) results in $x^2 \kappa^2 \cos^2 \phi = \tilde{\gamma}^2$ or, for a positive value of $\cos \phi$,

$$\frac{E_b}{E_a} = \frac{\Gamma_{\perp} + \Gamma_{\parallel} + 2\gamma'}{(\Gamma_{\perp} - \Gamma_{\parallel}) \cos \phi}, \tag{20}$$

provided that $\Gamma_{\perp} \neq \Gamma_{\parallel}$. In this case,

$$\text{Re}[\chi^{(1)}(\delta = 0)] = A \frac{\alpha}{\varepsilon} = \frac{N\mu'^2}{2\varepsilon_0\hbar} \frac{-\omega_{32} + (\Gamma_{\perp} + \Gamma_{\parallel} + 2\gamma') \tan \phi}{\frac{\omega_{32}^2}{4} + (\Gamma_{\parallel} + \gamma')(\Gamma_{\perp} + \gamma')}. \tag{21}$$

After that, we describe the requirements for achieving complete optical transparency, i.e., $[\chi^{(1)}(\delta) = 0]$. By using Equations (16) and (17), we can determine that this happens when $\beta = 0$ and $\delta = -\alpha$ or

$$\frac{E_b}{E_a} \cos \phi = \frac{\Gamma_{\perp} + \Gamma_{\parallel} + 2\gamma'}{\Gamma_{\perp} - \Gamma_{\parallel}}, \tag{22}$$

and

$$\delta = \frac{\omega_{32}}{2} - \frac{\Gamma_{\perp} - \Gamma_{\parallel}}{2} \frac{E_b}{E_a} \sin \phi. \tag{23}$$

This indicates that laser *a* can achieve complete optical transparency within the system, provided that Γ_{\perp} is different from Γ_{\parallel} . It is important to emphasize that this transparency is precise and not an approximation, and it remains unaffected by the vacuum decay rate γ' . This differs from the previous work where a single linearly polarized laser field was used to interact with the system [39].

In addition, when ϕ satisfying Equation (22), Equation (23) signifies complete optical transparency at

$$\delta = \frac{\omega_{32}}{2} - \frac{1}{2} \sqrt{(\Gamma_{\perp} - \Gamma_{\parallel})^2 \frac{E_b^2}{E_a^2} - (\Gamma_{\perp} + \Gamma_{\parallel} + 2\gamma')^2}. \tag{24}$$

If the value inside the square root is zero or positive (represented concisely as $\kappa^2 x^2 \geq \tilde{\gamma}^2$), then the system can always achieve total optical transparency.

At $\delta = 0$, complete optical transparency is achieved for

$$\tan \phi = \frac{\omega_{32}}{\Gamma_{\perp} + \Gamma_{\parallel} + 2\gamma'}, \tag{25}$$

and

$$\frac{E_b}{E_a} = \frac{\sqrt{\omega_{32}^2 + (\Gamma_{\perp} + \Gamma_{\parallel} + 2\gamma')^2}}{\Gamma_{\perp} - \Gamma_{\parallel}}. \tag{26}$$

When $\omega_{32} = 0$, it follows that $\phi = n\pi$ where n is an integer (0, 1, 2, etc.), and Equation (26) transforms into

$$\frac{E_b}{E_a} = \frac{\Gamma_{\perp} + \Gamma_{\parallel} + 2\gamma'}{\Gamma_{\perp} - \Gamma_{\parallel}}. \tag{27}$$

Assuming that γ' is zero and Γ_{\perp} is much larger than Γ_{\parallel} , the above expression gives $E_a \approx E_b$.

Furthermore, it is possible to attain amplification within the system without the need for inversion because the overwhelming majority of the population remains in state $|0\rangle$.

This amplification (gain) can be obtained within the system if the value of $\text{Im}[\chi^{(1)}(\tilde{\omega})]$ is negative and Equation (19) gives the necessary conditions for achieving gain without inversion. The range of δ values that provide gain without inversion lies between δ_- and δ_+ [Equation (18)], when $\kappa x \cos \phi + \tilde{\gamma}$ or

$$(\Gamma_{\perp} - \Gamma_{\parallel}) \frac{E_b}{E_a} \cos \phi + \Gamma_{\perp} + \Gamma_{\parallel} + 2\gamma' > 0. \tag{28}$$

In the situations we are considering, the condition $\cos \phi \geq 0$ is always met. When the expression $\kappa x \cos \phi + \tilde{\gamma}$ becomes negative, it becomes possible to achieve a gain that falls outside the interval defined by $[\delta_-, \delta_+]$.

4. Results and Discussion

To begin with, we consider that the QE stands alone in vacuum. The corresponding susceptibility can be seen in Figure 2. We observe that both the real and imaginary parts have the typical form of a Lorentzian-type susceptibility. Since the QE is in vacuum, there is no quantum interference in the system and therefore $\kappa = 0$ in Equation (14). This means that there no phase-dependent phenomena in this case as the susceptibility does not depend on ϕ .

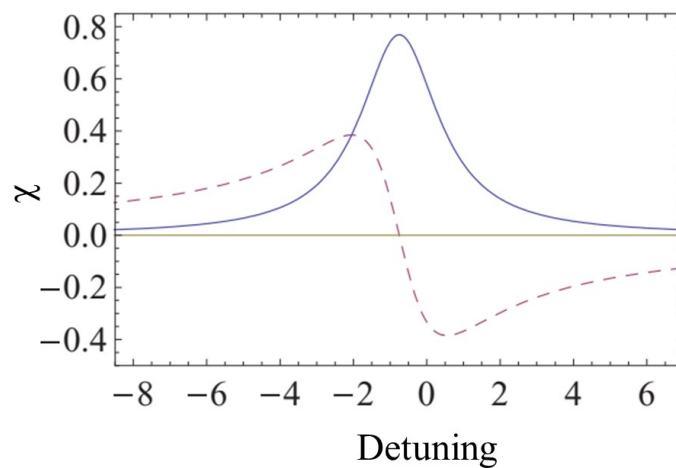


Figure 2. The graph depicting the absorption spectrum, represented by the solid curve of $\text{Im}(\chi^{(1)})$, and the dispersion spectrum, shown as the dashed curve of $\text{Re}(\chi^{(1)})$, is presented in normalized units $(N\mu'^2 / (\hbar\epsilon_0\Gamma_0))$, as described in Equation (14). The data correspond to the case where the QE is placed in vacuum. We assume that $\omega_{32} = 1.5\Gamma_0$, $\gamma' = 0.3\Gamma_0$, $E_b/E_a = 1.5$.

In Figure 3 we show the computational setup employed in order to highlight the exotic optical phenomena explained in the previous section. Namely, we assume that the double-V-type quantum emitter of Figure 1 is placed in the *middle* of a dimer of Bi_2Te_3 microspheres with $2 \mu\text{m}$ radius. By D we denote the distance between the two microspheres. Recent electromagnetic simulations [22] have shown that the double microsphere system can lead to a strong dependence of the SE rate on the orientation of a given atomic dipole relative to the surfaces of the microspheres (the anisotropic Purcell effect), which leads to high values for the quantum interference factor close to the maximum theoretical value of unity, at frequencies near the surface phonon-polariton frequencies of bismuth-chalcogenide microspheres. The high degree of quantum interference remains for a wide range of frequencies, namely from 8 to 16 THz and for various distances between the spheres [22].

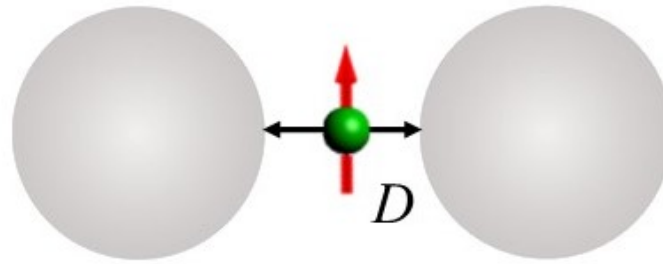


Figure 3. Computational setup: the double-V-type quantum emitter of Figure 1 is placed in the middle of a dimer of 2 μm Bi_2Te_3 microspheres.

The electromagnetic simulations are based on the finite element method [22] wherein the SE rate is calculated by means of the total power radiated (time-averaged Poynting vector) by the QE either in vacuum or in the presence of the Bi_2Te_3 microspheres according to the setup of Figure 3. The dielectric function of Bi_2Te_3 is provided as a sum of three Lorentzian-type terms [17],

$$\epsilon(\omega) = \sum_{j=\alpha,\beta,f} \frac{\omega_{pj}^2}{\omega_{0j}^2 - \omega^2 - i\gamma_j\omega} \quad (29)$$

where the subscripts indicate the contributions from α and β phonons, and bulk free-charge carriers f [17,40]. The dielectric function assumes very high values that are a result of the influence of phonon-polariton modes [16]. These modes introduce the necessary anisotropy in the spontaneous emission (SE) rates, varying for the two distinct dipole orientations and leading to the increased QI values.

Figure 4 shows absorption and dispersion spectra for different phases ϕ when the QE is placed in the middle of a Bi_2Te_3 microsphere dimer and for $\frac{E_b}{E_a} = 1.5$. Changing the phase ϕ strongly influences the shape of the absorption and dispersion spectra. Gain without inversion ($\text{Im}(\chi^{(1)}) < 0$) is obtained in all cases, with zero absorption ($\text{Im}(\chi^{(1)}) = 0$) and nonzero dispersion ($\text{Re}(\chi^{(1)}) \neq 0$). The detuning values where there is no absorption and the frequency range where gain occurs without inversion, vary as ϕ changes. This variation is attributed to how δ_{\pm} depends on the angle ϕ , as described in Equation (18).

In Figure 5, we display the absorption and dispersion spectra using the identical parameters as those employed in Figure 4, but this time for a larger gap between the microspheres, specifically for a gap size of $D = 4000 \mu\text{m}$, and a different QE frequency $\bar{\omega} = 14.1 \text{ THz}$. These parameters provide a degree of QI $p = 0.995$ which is even closer to the theoretical optimal value of unity than the value of Figure 4. We observe that similarly to Figure 4, in Figure 5 we also observe the same effects of zero absorption with nonzero dispersion and gain without inversion albeit with significantly different lineshapes for the corresponding real and imaginary parts of the susceptibility. This is due to the fact that in Figure 5, the separation (gap) between the Bi_2Te_3 microspheres is double the value used in Figure 4 and, naturally, the corresponding SE rates Γ_{\perp} and Γ_{\parallel} are much smaller than their counterparts of Figure 4. Nevertheless, the phase-related phenomena (zero absorption with nonzero dispersion and gain without inversion) are present which signifies that a precise tuning of the QE frequency or the accurate positioning of the microspheres to specific values are not prerequisite for their observation. This is important for a possible experimental demonstration of the numerical findings of the present work.

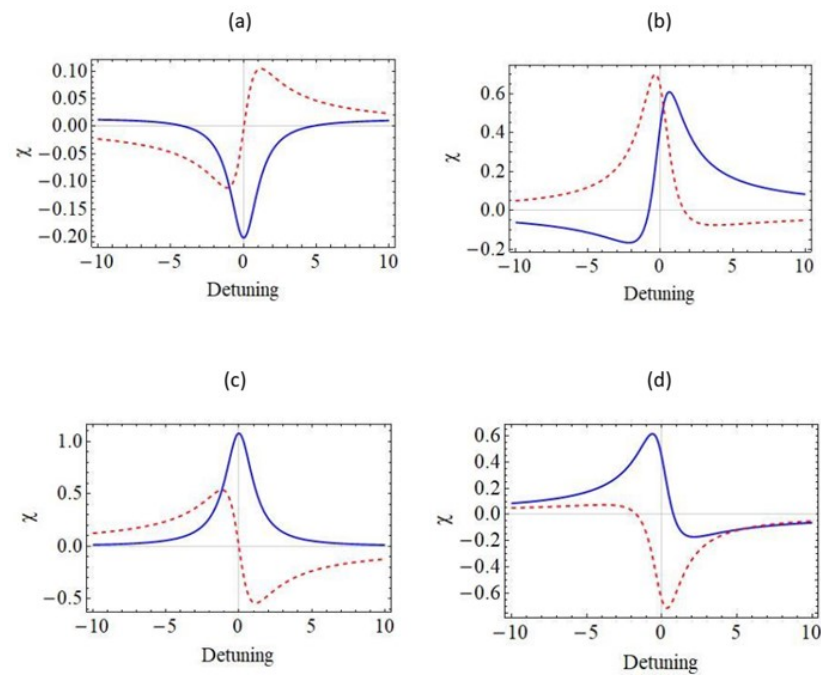


Figure 4. The graph depicting the absorption spectrum, represented by the solid curve of $\text{Im}(\chi^{(1)})$, and the dispersion spectrum, shown as the dashed curve of $\text{Re}(\chi^{(1)})$, is presented in normalized units ($N\mu'^2/(\hbar\epsilon_0\Gamma_0)$), as described in Equation (14). The data correspond to the computational configuration illustrated in Figure 3. We assume that $\omega_{32} = 1.5\Gamma_0$, $\gamma' = 0.3\Gamma_0$, $E_b/E_a = 1.5$. We have also chosen $\bar{\omega} = 12.43$ THz and the gap between the two microspheres to be $2000 \mu\text{m}$ so that $\Gamma_{\perp} = 88.51\Gamma_0$ and $\Gamma_{\parallel} = 0.851\Gamma_0$ which provide a degree of QI $p = 0.981$. In (a) $\phi = 0$, in (b) $\phi = \pi/2$, in (c) $\phi = \pi$, and in (d) $\phi = 3\pi/2$.

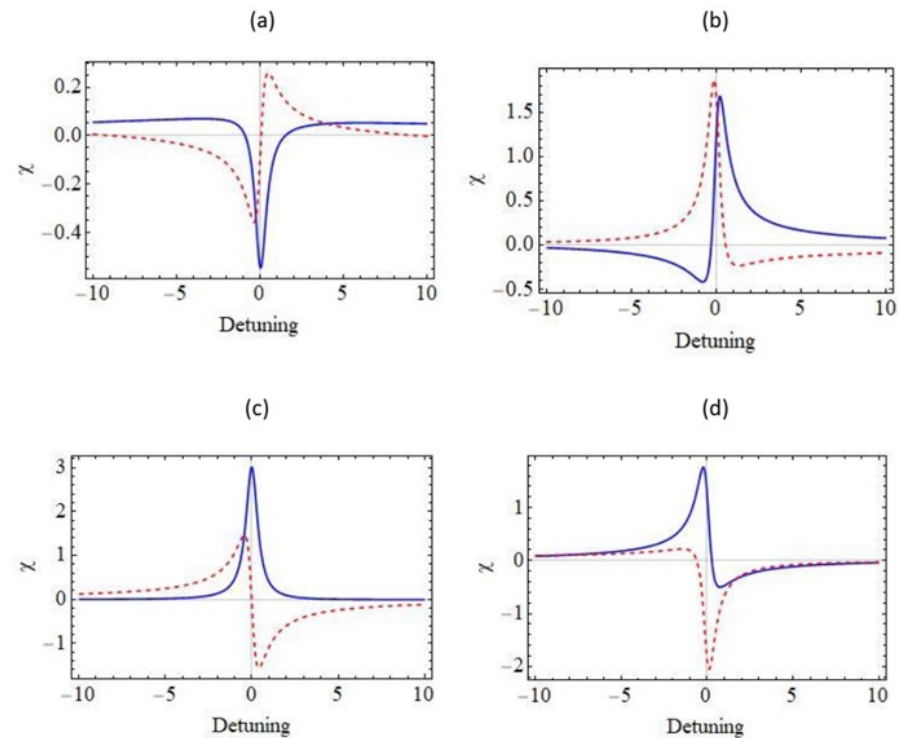


Figure 5. The same as Figure 4 but for a microsphere gap of $4000 \mu\text{m}$ and frequency $\bar{\omega} = 14.1$ THz which provide $\Gamma_{\perp} = 17.95\Gamma_0$ and $\Gamma_{\parallel} = 0.083\Gamma_0$ yielding a degree of QI $p = 0.995$.

Next, in Figure 6 we choose the phase ϕ such that it satisfies the conditions for total optical transparency, namely Equations (25) and (26). Under these conditions, we obtain vanishing real and imaginary parts of the susceptibility at exactly zero detuning, as it is evident from Figure 6. Figure 7 is similar to Figure 6 but for a 4 μm distance between the microspheres. We observe that the occurrence of a high degree of QI for this microsphere gap, too, ensures that by meeting the conditions (25) and (26) for the phase ϕ , one can actually achieve total transparency for the QE in study. We note that, in addition to the occurrence of complete optical transparency, Figures 6 and 7 exhibit zero absorption with nonzero dispersion at different frequencies and gain without inversion.

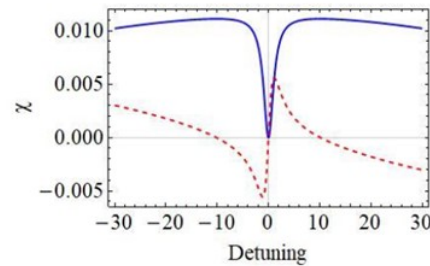


Figure 6. The same as Figure 4 but for ϕ satisfying Equations (25) and (26).

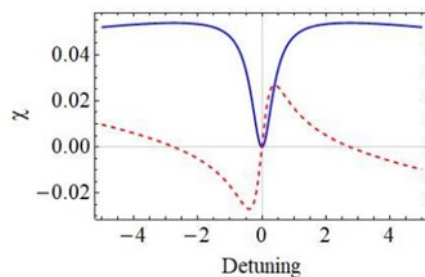


Figure 7. The same as Figure 6 but for a 4 μm gap between the microspheres.

As we conclude this section, we present some possibilities for experimentally realizing the double-V-type quantum system studied in this work. The system can be realized in different atomic systems, where transitions between $|2\rangle$ and $|1\rangle$ or $|0\rangle$, and between $|3\rangle$ and $|1\rangle$ or $|0\rangle$, have orthogonal matrix elements. One such possible realization involves using two $J = 0$ states for the lower states $|0\rangle$ and $|1\rangle$, and $M = \pm 1$ sublevels of a $J = 1$ state for the excited states $|2\rangle$ and $|3\rangle$. By applying a static magnetic field, the energy difference $\hbar\omega_{32}$ between states $|3\rangle$ and $|2\rangle$ can be adjusted. Typical quantum emitters for obtaining these effects in the THz regime rely on intersubband transitions of quantum wells and on intersublevel transitions of quantum dots [41]. Apart from that, electrons in highly-excited atomic Rydberg states orbit at THz frequencies whilst small molecules rotate at THz frequencies.

We note that the enhanced phase-dependent effects reported here can find application in various technological fields. Namely, the ability to efficiently control the absorption and dispersion properties of a quantum system using laser fields could lead to the development of highly efficient optical switches and modulators. By manipulating the electric field amplitudes and phase difference of the laser fields, it might be possible to control the transmission of light through a medium, enabling fast and precise modulation of optical signals. Moreover, the concept of zero absorption with nonzero dispersion suggests the possibility of generating slow and fast light effects. Slow light can be used for delaying optical signals, which could have applications in optical data buffering and storage. Fast light, on the other hand, could be used to accelerate optical signals and enhance signal processing capabilities. Lastly, the manipulation of quantum states through the control of absorption and dispersion properties could have implications for quantum information processing.

5. Conclusions

We have studied how a four-level quantum system, with two V-type transitions, interacts with two circularly polarized laser fields of the same frequency but different phases and electric field amplitudes, in the presence of nearby bismuth-chalcogenide microparticles. One transition is influenced by the presence of the surface phonon-polariton excitations of the microspheres while the other interacts with free-space vacuum. By using density matrix methodology, we found that the presence of bismuth-chalcogenide microspheres modifies the absorption and dispersion spectra of one laser field in the presence of the other. We also discovered that by adjusting the phase difference and electric field amplitudes of the two laser fields, we can control the optical properties of the system and achieve exotic phenomena such as optical transparency, zero absorption with non-zero dispersion, and gain without inversion.

Author Contributions: Methodology, T.P., V.Y. and E.P.; software, N.K.; validation, N.K., V.Y. and E.P.; investigation, T.P., V.Y., N.K. and E.P.; resources, E.P. and V.Y.; data curation, T.P.; writing—original draft preparation, V.Y.; writing—review and editing, N.K., V.Y., T.P. and E.P.; visualization, V.Y.; supervision, V.Y. All authors have read and agreed to the published version of the manuscript.

Funding: The Center for Polariton-driven Light–Matter Interactions (POLIMA) is sponsored by the Danish National Research Foundation (Project No. DNRF165).

Institutional Review Board Statement: Not applicable.

Informed Consent Statement: Not applicable.

Data Availability Statement: The data presented in this study are available on reasonable request from the corresponding author

Conflicts of Interest: The authors declare no conflict of interest.

References

1. Tame, M.S.; McEnery, K.R.; Özdemir, Ş.K.; Lee, J.; Maier, S.A.; Kim, M.S. Quantum plasmonics. *Nat. Phys.* **2013**, *9*, 329. [[CrossRef](#)]
2. Lodahl, P.; Mahmoodian, S.; Stobbe, S. Interfacing single photons and single quantum dots with photonic nanostructures. *Rev. Mod. Phys.* **2015**, *87*, 347. [[CrossRef](#)]
3. Hohenester, U. *Nano and Quantum Optics: An Introduction to Basic Principles and Theory*; Springer: Cham, Switzerland, 2019.
4. Tserkezis, C.; Fernandez-Dominguez, A.I.; Dias Gonçalves, P.A.; Todisco, F.; Cox, J.D.; Busch, K.; Stenger, N.; Bozhevolnyi, S.I.; Mortensen, N.A.; Wolff, C. On the applicability of quantum-optical concepts in strong-coupling nanophotonics. *Rep. Prog. Phys.* **2020**, *83*, 082401. [[CrossRef](#)] [[PubMed](#)]
5. Schuller, J.A.; Barnard, E.S.; Cai, W.; Jun, Y.C.; White, J.S.; Brongersma, M.L. Plasmonics for extreme light concentration and manipulation. *Nat. Mater.* **2010**, *9*, 193. [[CrossRef](#)]
6. Baranov, D.G.; Wersäll, M.; Cuadra, J.; Antosiewicz, T.J.; Shegai, T. Novel Nanostructures and Materials for Strong Light–Matter Interactions. *ACS Photonics* **2018**, *5*, 24. [[CrossRef](#)]
7. Purcell, E.M. Spontaneous emission probabilities at radio frequencies. *Phys. Rev.* **1946**, *69*, 681.
8. Drexhage, K.H. Influence of a dielectric interface on fluorescence decay time. *J. Lumin.* **1970**, *1*, 693–701. [[CrossRef](#)]
9. Drexhage, K.H. Interaction of light with monomolecular dye lasers. *Prog. Opt.* **1974**, *12*, 163–232.
10. West, P.R.; Ishii, S.; Naik, G.V.; Emani, N.K.; Shalaev, V.M.; Boltasseva, A. Searching for better plasmonic materials. *Laser Photonics Rev.* **2010**, *4*, 795. [[CrossRef](#)]
11. Naik, G.V.; Shalaev, V.M.; Boltasseva, A. Alternative plasmonic materials: Beyond gold and silver. *Adv. Mater.* **2013**, *25*, 3264. [[CrossRef](#)]
12. Kinsey, N.; Ferrera, M.; Shalaev, V.M.; Boltasseva, A. Examining nanophotonics for integrated hybrid systems: A review of plasmonic interconnects and modulators using traditional and alternative materials. *J. Opt. Soc. Am. B Opt. Phys.* **2015**, *32*, 121. [[CrossRef](#)]
13. Xia, C.; Li, J. Recent advances in optoelectronic properties and applications of two-dimensional metal chalcogenides. *J. Semicond.* **2016**, *37*, 051001. [[CrossRef](#)]
14. You, J.W.; Bongu, S.R.; Bao, Q.; Panoui, N.C. Nonlinear optical properties and applications of 2D materials: Theoretical and experimental aspects. *Nanophotonics* **2018**, *8*, 63. [[CrossRef](#)]
15. Mandal, A.; Cui, Y.; McRae, L.; Gholipour, B. Reconfigurable chalcogenide phase change metamaterials: A material, device, and fabrication perspective. *J. Phys. Photonics* **2021**, *3*, 022005. [[CrossRef](#)]
16. Siroki, G.; Lee, D.; Haynes, P. Single-electron induced surface plasmons on a topological nanoparticle. *Nat. Commun.* **2016**, *7*, 12375. [[CrossRef](#)]

17. Rider, M.S.; Sokolikova, M.; Hanham, S.M.; Navarro-Cia, M.; Haynes, P.D.; Lee, D.K.K.; Daniele, M.; Guidi, M.C.; Mattevi, C.; Lupi, S.; et al. Experimental signature of a topological quantum dot. *Nanoscale* **2020**, *12*, 22817–22825. [[CrossRef](#)]
18. Kianinia, M.; Xu, Z.-Q.; Toth, M.; Aharonovich, I. Quantum emitters in 2D materials: Emitter engineering, photophysics, and integration in photonic nanostructures. *Appl. Phys. Rev.* **2022**, *9*, 011306. [[CrossRef](#)]
19. Colas des Francs, G.; Barthes, J.; Bouhelier, A.; Weeber, J.C.; Dereux, A.; Cuche, A.; Girard, C. Plasmonic Purcell factor and coupling efficiency to surface plasmons. Implications for addressing and controlling optical nanosources. *J. Opt.* **2016**, *18*, 094005. [[CrossRef](#)]
20. Chatzidakis, G.D.; Yannopapas, V. Strong electromagnetic coupling in dimers of topological-insulator nanoparticles and quantum emitters. *Phys. Rev. B* **2020**, *101*, 165410. [[CrossRef](#)]
21. Karaoulanis, D.; Paspalakis, E.; Yannopapas, V. Quantum interference near bismuth-chalcogenide microstructures. *J. Opt. Soc. Am. B* **2021**, *38*, 3301–3308. [[CrossRef](#)]
22. Kyvelos, N.; Tsigaridas, G.; Paspalakis, E.; Yannopapas, V. Quantum Interference in Spontaneous Decay of a Quantum Emitter Placed in a Dimer of Bismuth-Chalcogenide Microparticles. *Photonics* **2022**, *9*, 596. [[CrossRef](#)]
23. Vladimirova, Y.V.; Zadkov, V.N. Quantum Optics in Nanostructures. *Nanomaterials* **2021**, *11*, 1919. [[CrossRef](#)] [[PubMed](#)]
24. Paspalakis, E.; Evangelou, S.; Yannopapas, V.; Terzis, A.F. Phase-dependent optical effects in a four-level quantum system near a plasmonic nanostructure. *Phys. Rev. A* **2013**, *88*, 053832. [[CrossRef](#)]
25. Carreño, F.; Antón, M.A.; Yannopapas, V.; Paspalakis, E. Control of the absorption of a four-level quantum system near a plasmonic nanostructure. *Phys. Rev. B* **2017**, *95*, 195410. [[CrossRef](#)]
26. Javanmard, M. Two-dimensional plasmon induced grating in a double V-type quantum system. *Laser Phys.* **2020**, *30*, 125201. [[CrossRef](#)]
27. Ranjbar, A.H.; Mortezapour, A. Electromagnetically induced gain-phase grating in a double V-type quantum system. *J. Opt. Soc. Am. A* **2019**, *36*, 549–555. [[CrossRef](#)]
28. Evangelou, S.; Yannopapas, V.; Paspalakis, E. Modifying free space spontaneous emission near a plasmonic nanostructure. *Phys. Rev. A* **2011**, *83*, 023819. [[CrossRef](#)]
29. Agarwal, G.S. Anisotropic Vacuum-Induced Interference in Decay Channels. *Phys. Rev. Lett.* **2000**, *84*, 5500. [[CrossRef](#)]
30. Kiffner, M.; Macovei, M.; Evers, J.; Keitel, C.H. *Progress in Optics*; Wolf, E., Ed.; 2010 ; Volume 55, p. 85.
31. Li, G.X.; Li, F.-L.; Zhu, S.-Y. Quantum interference between decay channels of a three-level atom in a multilayer dielectric medium. *Phys. Rev. A* **2001**, *64*, 013819. [[CrossRef](#)]
32. Yang, Y.-P.; Xu, J.-P.; Chen, H.; Zhu, S.-Y. Quantum Interference Enhancement with Left-Handed Materials. *Phys. Rev. Lett.* **2008**, *100*, 043601. [[CrossRef](#)]
33. Li, G.-X.; Evers, J.; Keitel, C.H. Spontaneous emission interference in negative-refractive-index waveguides. *Phys. Rev. B* **2009**, *80*, 045102. [[CrossRef](#)]
34. Xu, J.-P.; Yang, Y.-P. Quantum interference of V-type three-level atom in structures made of left-handed materials and mirrors. *Phys. Rev. A* **2010**, *81*, 013816. [[CrossRef](#)]
35. Bortman-Arbiv, D.; Wilson-Gordon, A.D.; Friedmann, H. Phase control of group velocity: From subluminal to superluminal light propagation. *Phys. Rev. A* **2001**, *63*, 043818. [[CrossRef](#)]
36. Ficek, Z.; Swain, S. *Quantum Interference and Coherence: Theory and Experiments*; Springer: New York, NY, USA, 2005.
37. Scully, M.O. Enhancement of the index of refraction via quantum coherence. *Phys. Rev. Lett.* **1991**, *67*, 1855. [[CrossRef](#)]
38. Fleischhauer, M.; Keitel, C.H.; Scully, M.O.; Su, C.; Ulrich, B.T.; Zhu, S.-Y. Resonantly enhanced refractive index without absorption via atomic coherence. *Phys. Rev. A* **1992**, *46*, 1468. [[CrossRef](#)] [[PubMed](#)]
39. Evangelou, S.; Yannopapas, V.; Paspalakis, E. Transparency and slow light in a four-level quantum system near a plasmonic nanostructure. *Phys. Rev. A* **2012**, *86*, 053811. [[CrossRef](#)]
40. Pelton, M. Modified spontaneous emission in nanophotonic structures. *Nat. Photonics* **2015**, *9*, 427–435. [[CrossRef](#)]
41. Harrison, P.; Valavanis, A. *Quantum Wells, Wires and Dots*, 4th ed.; Wiley: Hoboken, NJ, USA, 2016.

Disclaimer/Publisher’s Note: The statements, opinions and data contained in all publications are solely those of the individual author(s) and contributor(s) and not of MDPI and/or the editor(s). MDPI and/or the editor(s) disclaim responsibility for any injury to people or property resulting from any ideas, methods, instructions or products referred to in the content.